Journal of Computational Physics 229 (2010) 4855–4868

Contents lists available at ScienceDirect

Journal of Computational Physics

journal homepage: www.elsevier.com/locate/jcp

Short Note

On reducing interface curvature computation errors in the height function technique

J. López [a], J. Hernández [b,*]

[a] Dept. de Ingeniería de Materiales y Fabricación, ETSII, Universidad Politécnica de Cartagena, E-30202 Cartagena, Spain
[b] Dept. de Mecánica, ETSII, UNED, E-28040 Madrid, Spain

ARTICLE INFO

Article history:
Received 25 September 2009
Received in revised form 23 March 2010
Accepted 23 March 2010
Available online 30 March 2010

Keywords:
Volume of fluid method
Level set method
Height function technique
Interface curvature

ABSTRACT

A detailed analysis of the errors involved in computing the interface curvature from volume fraction distributions using a height function technique is presented. An improved version of the height function technique is proposed, based on introducing a correction of the height function discretization error estimated from the local osculating spheres at interface points. By using this error correction and an appropriate discretization of the partial derivatives of the height function, a substantial improvement in the accuracy of the interface curvature computation can be efficiently achieved.

1. Introduction

Increasingly, in recent years, the height function (HF) technique has been used to compute interface curvature from volume of fluid (VOF) fractions [4,6,9,1,10,14–16,18,22] because of its relatively easy implementation, good computational efficiency and second-order accuracy. In this technique, the interface curvature is calculated from the derivatives of the fluid heights constructed by integrating the discretized VOF function, F, along the direction of the largest component of the interface normal vector. Recent improvements of the HF technique include the development of a systematic approach for calculating curvature from volume fractions which is accurate to any order [19], the extension to non-uniform rectangular grids [7], and the development of a height function technique for computing curvature from the level set function [20].

In this work, a detailed analysis of the errors involved in the HF technique is carried out in an attempt to minimize them and increase the accuracy of curvature computation. The paper is organized as follows. The HF technique incorporating the adaptive stencil proposed in [10] and improved discretization of the partial derivatives of the HF proposed in [14] is briefly described in Section 2. Then, a detailed assessment of the errors involved in the HF technique is carried out in Section 3. Finally, an improved version of the HF technique, based on a simple error correction model, is presented in Section 4 followed by a comparison of the results with those obtained with previous versions (Section 5).

2. Height function technique

Let us consider an interfacial cell, (i,j,k), where $0 < F < 1$, in which the absolute value of the z component of the interface normal vector, $\boldsymbol{n}$, is largest (at this point of the study $\boldsymbol{n}$ will be obtained from the gradient of the volume fraction function, ∇F,

* Corresponding author. Tel.: +34 91 398 6424; fax: +34 91 398 6536.
E-mail addresses: joaquin.lopez@upct.es (J. López), jhernandez@ind.uned.es (J. Hernández).

0021-9991/$ - see front matter © 2010 Elsevier Inc. All rights reserved.
doi:10.1016/j.jcp.2010.03.032

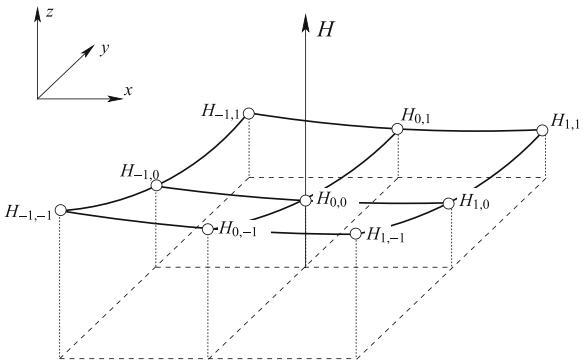

Fig. 1. κ-stencil for height function calculation.

using the method of Youngs [24]). Using a 3×3 stencil centered at cell (i,j,k) (Fig. 1) on the xy plane (referred to hereafter as the κ-stencil), a local distribution of a height function, H, is calculated as follows:

$$H^{\mathrm{VOF}}_{r,s} = \sum_{t=-t_{\mathrm{down}}}^{t_{\mathrm{up}}} F^{*}_{i+r,j+s,k+t} h, \quad \text{for } r=-1,0,1 \quad \text{and} \quad s=-1,0,1, \tag{1}$$

where t_{down} and t_{up} are adaptatively adjusted from 0 to 3 as indicated in [10], h is the cell size and F^{*} is a modified distribution of the volume fraction, F, which is forced to follow a local monotonic variation along the z direction [10]. Note that the $3 \times 3 \times (t_{\mathrm{down}} + t_{\mathrm{up}} + 1)$ stencil surrounding cell (i,j,k) is adaptively adjusted from $3 \times 3 \times 1$ to $3 \times 3 \times 7$ cells, depending on the local grid resolution (a detailed description of the adaptive stencil can be found in [10]). The superscript VOF is used in the height function of Eq. (1) to differentiate it from the exact and approximate height functions defined in the following sections. For two-dimensional problems, the above procedure can be derived in a straightforward way, and only specific considerations needed for such geometries will be mentioned.

The curvature of the interface is determined from the height function H as

$$\kappa = \frac{H_{xx} + H_{yy} + H_{xx}H_y^2 + H_{yy}H_x^2 - 2H_{xy}H_xH_y}{\left(1 + H_x^2 + H_y^2\right)^{3/2}}, \tag{2}$$

where the partial derivatives of H are obtained using the finite difference formula proposed by López et al. [14], which considerably improves the curvature accuracy in three-dimensional problems. For example, the derivatives H_x and H_{xx} (as in the y-direction) are obtained as [14]

$$H_x = [\gamma(H_{1,1} - H_{-1,1}) + H_{1,0} - H_{-1,0} + \gamma(H_{1,-1} - H_{-1,-1})]/2h(1+2\gamma), \tag{3}$$

$$H_{xx} = [\gamma(H_{1,1} - 2H_{0,1} + H_{-1,1}) + H_{1,0} - 2H_{0,0} + H_{-1,0} + \gamma(H_{1,-1} - 2H_{0,-1} + H_{-1,-1})]/h^2(1+2\gamma), \tag{4}$$

where the "smoother" parameter γ is defined as

$$\gamma = \begin{cases} 0.0 & \text{if } \theta < 0.8 \text{ rad} \\ 0.2 & \text{otherwise,} \end{cases} \tag{5}$$

with $\theta = \arccos[\max(|n_x|,|n_y|,|n_z|)]$. Note that a constant value of γ equal to 0.0 produces a standard second-order finite difference approximation, and that the smoothing can only be applied to 3D cases [14]. The cross derivative H_{xy} is calculated as

$$H_{xy} = (H_{1,1} - H_{1,-1} - H_{-1,1} + H_{-1,-1})/4h^2. \tag{6}$$

3. Assessment of errors in the height function technique

The errors involved in computing the interface curvature from volume fractions using a height function technique mainly arise from discretization of the height function and its partial derivatives. Another source of errors that may compromise accuracy is the initialization of the volume fraction distribution. To reduce initialization errors, we use the accurate procedure described in [14], with $n_{\mathrm{sc}} = 16$ (n_{sc}^2 in 2D and n_{sc}^3 in 3D are the numbers of sub-cells into which every interfacial cell is subdivided to compute the initial F distribution), and the routines supplied in [25] (see also Ref. [13]).

3.1. Height function discretization error

We will first consider the circular interface of Fig. 2, with radius $R = 1$ and center of curvature located at $(x, y) = (A, 0)$, and assume that the largest component of the interface normal vector at $x = 0$ is along the y axis, so that $-R/\sqrt{2} < A < R/\sqrt{2}$. For a given grid with cell size h, the error introduced when using a discretized height function to define the location of the interface at $x = 0$ is given by

$$\xi = H^h - H^{\text{exact}}, \tag{7}$$

where $H^{\text{exact}} = (R^2 - A^2)^{1/2}$ is the exact height function at $x = 0$ and H^h is the approximate height function for the discrete column of size h aligned with the y-axis,

$$H^h = \frac{1}{h}\int_{-h/2}^{h/2} [R^2 - (x - A)^2]^{1/2}\,\mathrm{d}x. \tag{8}$$

Fig. 3(a) shows the increase in the height function discretization error, $|\xi|$, obtained analytically for different grid cell sizes, with an increasing angle between the interface normal vector and the y axis, $\theta = \arccos|n_y| = \arccos\frac{(R^2-A^2)^{1/2}}{R}$. The error $|H^{\text{VOF}} - H^{\text{exact}}|$ has also been computed at all the grid cells crossed by the circular interface, centered in a domain of size 8^2, and represented by open circles in Fig. 3(a). The angle θ is now defined as $\theta = \arccos[\max(|n_x|, |n_y|)]$, where the interface

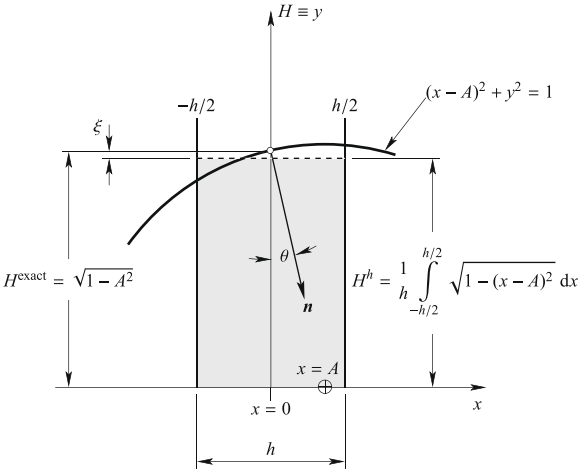

Fig. 2. Approximate height function calculation for a circular interface with $R = 1$.

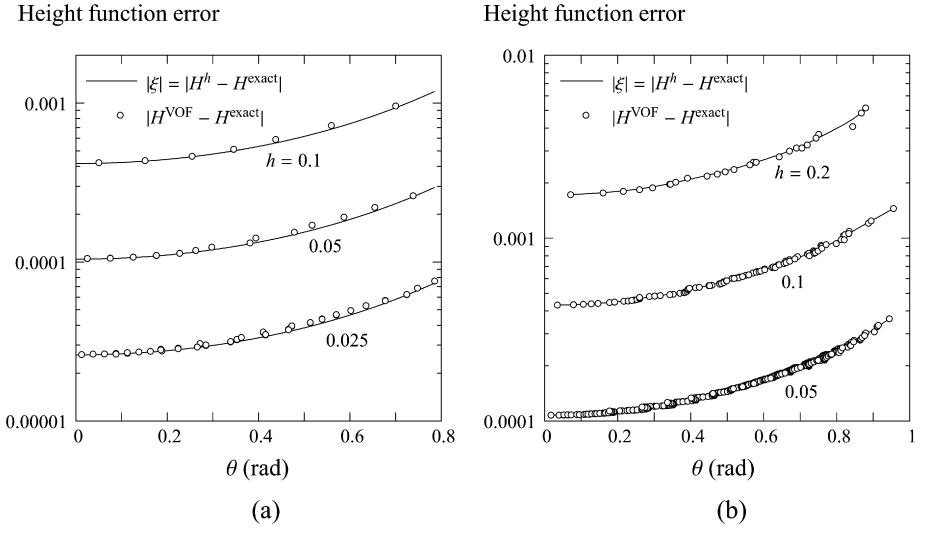

Fig. 3. Height function errors as a function of θ for different grid resolutions: (a) circular interface with $R = 1$ and (b) spherical interface with $R = 2$.

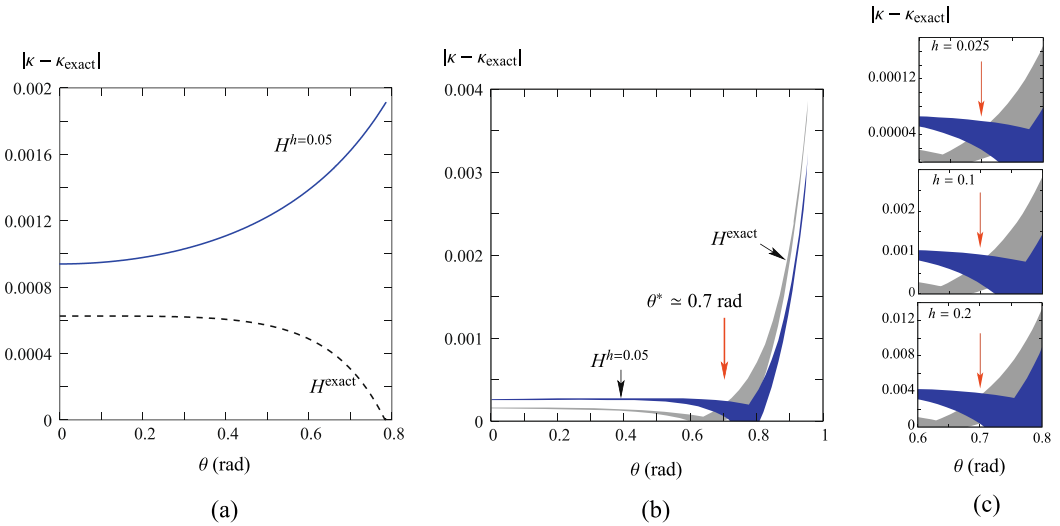

Fig. 4. Interface curvature errors obtained from the approximate and exact height function distributions, H^h and H^{exact}, using standard second-order finite difference approximations ($\gamma = 0$ in Eqs. (3) and (4)), with a grid cell size $h = 0.05$: (a) circular interface of radius unity, (b) spherical interface of radius 2 and (c) detailed results of the 3D case obtained with different grid sizes.

orientation is obtained using Youngs' method [24]. Note that the small differences between the two errors represented in Fig. 3(a) are only due to the errors introduced in the volume fraction initialization procedure and in the interface orientation calculation.

A similar analysis can be made in three dimensions (3D), considering a spherical interface of radius R and center of curvature located at $(A, B, 0)$, and assuming that, at $x = 0$ and $y = 0$, $|n_z| > |n_x|$ and $|n_z| > |n_y|$, so that the conditions $-(R^2 - B^2)^{1/2}/\sqrt{2} < A < (R^2 - B^2)^{1/2}/\sqrt{2}$ and $-(R^2 - A^2)^{1/2}/\sqrt{2} < B < (R^2 - A^2)^{1/2}/\sqrt{2}$ are satisfied. Writing the expression equivalent to Eq. (8) in 3D is straightforward and $H^{\text{exact}} = (R^2 - A^2 - B^2)^{1/2}$ at $x = 0$ and $y = 0$.

Results for $|\xi|$ similar to those of Fig. 3(a), obtained for $R = 2$ and three different grid sizes, are depicted by solid lines in Fig. 3(b). The angle θ between the interface normal vector and the z axis at $x = 0$ and $y = 0$ is given by $\theta = \arccos|n_z| = \arccos\frac{(R^2 - A^2 - B^2)^{1/2}}{R}$. The error $|H^{\text{VOF}} - H^{\text{exact}}|$, computed at all the interfacial cells from the initialized fluid volume fraction distribution for a spherical interface centered in a domain of 8^3, is also represented in Fig. 3(b). The angle θ is now defined as $\theta = \arccos[\max(|n_x|, |n_y|, |n_z|)]$ (note that the maximum angle formed between the height function direction and the interface normal vector is of 0.955 rad (54.74°) in 3D and of 0.785 rad (45°) in 2D). As in the 2D case, the errors increase as θ increases, and the height function H^{VOF} remains second-order accurate for any value of θ provided that an accurate initialization of the volume of fluid fraction is used.

Obviously, the height function discretization error could be reduced if the height function direction at every interfacial cell were made coincident with the interface normal vector direction (in the case of a circular interface, this error would be $\xi = 1 - \frac{1}{2}\left[1 - \left(\frac{h}{2}\right)^2\right]^{1/2} - \frac{1}{h}\arcsin\frac{h}{2}$). However, this would not be a simple task when a fixed Cartesian grid is used. A simpler procedure that significantly reduces the effect of the height function discretization error on curvature accuracy, and which is easy to implement, is proposed in Section 4.

3.2. Interface curvature errors

The interface curvature errors obtained from the approximate H^h distribution, using standard second-order finite difference approximations ($\gamma = 0$ in Eqs. (3) and (4)), for $h = 0.05$ and circular and spherical interfaces, are represented in Fig. 4(a) (solid line) and Fig. 4(b) (blue shaded area), respectively. In order to evaluate separately the influence of the discretization error of the partial derivatives of the height function on the interface curvature accuracy, the curvature error obtained from H^{exact} (dashed line in Fig. 4(a) and grey shaded area in Fig. 4(b)) are also represented in the figure (results similar to those of Fig. 4(b) are also represented in Fig. 4(c) for different grid resolutions).[1] The variable width of the blue and grey shaded areas in Fig. 4(b) and (c) are due to the different values that the lowest and intermediate components of the interface normal vector can take for a given θ value. Note that the discretization errors of the derivatives of the height function for highly inclined interfaces in 3D make the curvature errors for the highest value of θ about one order of magnitude larger than those for low θ values. Also note that for highly inclined interfaces in 3D (values larger than around of 0.7 rad)

[1] For interpretation of references to color in Fig. 4, the reader is referred to the web version of this article.

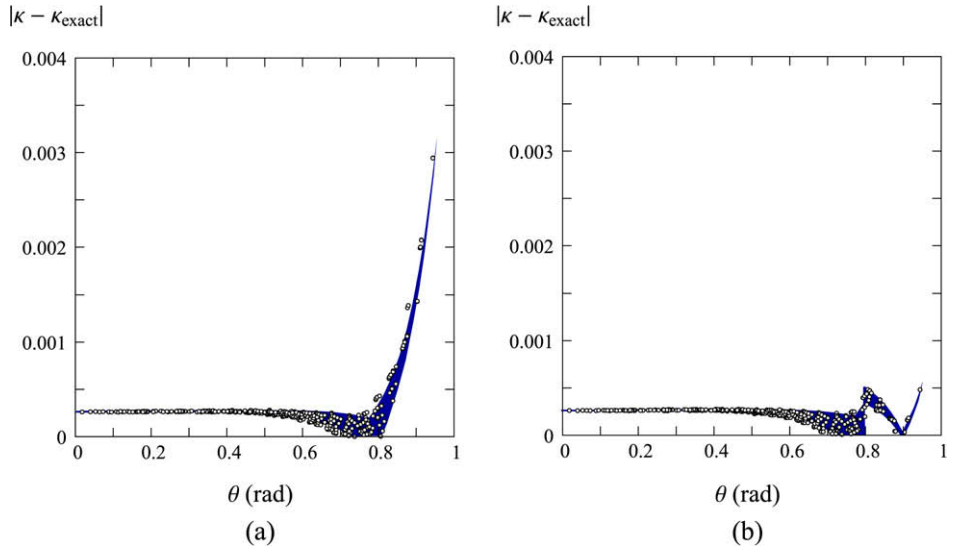

Fig. 5. Interface curvature errors obtained from the height function distribution H^{VOF} with a grid cell size $h = 0.05$, for a spherical interface of radius 2 (open circles): (a) standard second-order finite difference approximations ($\gamma = 0$ in Eqs. (3) and (4)) and (b) smoothed finite difference approximations (γ from Eq. (5)). The blue shaded areas denote the corresponding errors obtained from the approximate distribution H^h. (For interpretation of references to color in this legend Fig. 5, the reader is referred to the web version of this article.)

the discretization errors of the partial derivatives of the height function make the curvature errors obtained from the exact height function H^{exact} even greater than those obtained from the approximate height function. Similar results are found for other grid resolutions (see Fig. 4(c)). On the other hand, in 2D, and for the grid resolutions considered in this work, the curvature errors obtained from H^{exact} were always lower than those obtained from the approximate height function for any value of θ (as in the example of Fig. 4(a)).

Curvature errors in 3D are considerably reduced when the discretization of the partial derivatives of H proposed in [14] is used. Fig. 5(a) and (b) shows the interface curvature errors obtained from the approximate height function given by the equation equivalent to Eq. (8) in 3D (blue shaded areas) and from the volume fraction distribution (open circles), using, respectively, $\gamma = 0$ and γ given by Eq. (5) in Eqs. (3) and (4). Note that a considerable improvement in the curvature accuracy for highly inclined interfaces is obtained when the smoothed approximations are used for the partial derivatives of H.

4. Proposed method to improve accuracy in the interface curvature computation

A further improvement in the interface curvature computation can be achieved if the approximate height function obtained from the volume fraction distribution, H^{VOF}, is corrected by subtracting the error ξ, defined as in Eq. (7), corresponding to the local osculating spheres (circles in 2D) constructed at the interface points. This correction is motivated by the excellent agreement observed in Fig. 3 between ξ, obtained analytically, and the error $H^{VOF} - H^{exact}$. Although not in the context of the HF technique, various authors have used a similar *a priori* prescription of underlying interface shapes (such as circles [3], parabolas [17] and cubic splines [8,12,5]) in the curvature model. The possible advantages of using different interface shapes in curvature correction will be investigated in future studies.

In 3D, the corrected local distribution of the height function at a given interfacial cell (i,j,k) is obtained as

$$H_{r,s}^{VOF(*)} = \begin{cases} H_{r,s}^{VOF} - \xi_{r,s}, & \text{if } \theta < 0.7 \text{ rad} \\ H_{r,s}^{VOF}, & \text{otherwise,} \end{cases} \tag{9}$$

for $r = -1, 0, 1$ and $s = -1, 0, 1$ (in 2D, $H_r^{VOF(*)} = H_r^{VOF} - \xi_r$ for any value of θ). The limiting value of θ in Eq. (9) is adopted because of the lower curvature accuracy obtained when the exact height function is used instead of H^{VOF} for θ values larger than about 0.7 rad (Fig. 4(b) and (c)). The correction term $\xi_{r,s}$ is calculated as

$$\xi_{r,s} = \frac{2}{\kappa_{r,s} h^2} \int_{-h/2}^{h/2} \int_{-h/2}^{h/2} \left[1 - \left(\frac{\kappa_{r,s}}{2} x + n_{x(r,s)} \right)^2 - \left(\frac{\kappa_{r,s}}{2} y + n_{y(r,s)} \right)^2 \right]^{1/2} dx\, dy - \frac{2}{\kappa_{r,s}} \left(1 - n_{x(r,s)}^2 - n_{y(r,s)}^2 \right)^{1/2}, \tag{10}$$

where the first term on the right hand side is the approximate height function, defined as in an equation equivalent to Eq. (8) in 3D, and the second term is the exact height function of the osculating sphere of radius $2/|\kappa_{r,s}|$ (osculating circle of radius $1/|\kappa_r|$ in 2D) at the interface point (curvature $\kappa_{r,s}$ is negative when the center of curvature lies in the fluid), with orientation given by $(n_{x(r,s)}, n_{y(r,s)}, n_{z(r,s)})$. Note that the x and y coordinates of the osculating sphere center relative to the cell center

$(i+r, j+s, k)$ (parameter A in Eq. (8) and in the 2D example of Fig. 2) can be expressed as $-\frac{2}{\kappa_{r,s}} n_{x(r,s)}$ and $-\frac{2}{\kappa_{r,s}} n_{y(r,s)}$, respectively. The integral in Eq. (10) is calculated using a 5-point Gauss–Legendre procedure, which provides sufficient accuracy, instead of using an analytical procedure.

When the direction of the maximum component of the vector normal to the interface (the height function direction) does not change over all the interface points of the κ-stencil of Fig. 1 (a general occurrence, except in highly inclined interfaces), the interface curvature and normal vector used to obtain the correction term $\xi_{r,s}$ are estimated from the local height function distribution H^{VOF} at the interfacial cell $(i+r, j+s, k+t_{r,s})$, with $t_{r,s} = -\text{sign}(n_z)[\text{int}(H_{0,0}/h) - \text{int}(H_{r,s}/h)]$, using standard second-order finite difference approximations for the partial derivatives of H^{VOF}. When the previous condition does not hold, the interface orientation is obtained as $n_{x(r,s)} = n_{x(0,0)} + rh\kappa_{0,0}/2$ and $n_{y(r,s)} = n_{y(0,0)} + sh\kappa_{0,0}/2$ (in 2D, $n_{x(r)} = n_{x(0)} + rh\kappa_0$), and the curvature $\kappa_{r,s} = \kappa_{0,0}$.

The extension of the proposed method to non-uniform rectangular grids, which is beyond the scope of this work, could be accomplished by taking into account the approach recently proposed by Francois and Swartz [7].

In order to investigate the dependence of the proposed height function technique on the interface tracking scheme used, we have implemented, following the idea proposed in [20], a version in which the height function is computed from the distance function to the interface, which may be useful in level set methods. In Appendix A we briefly introduce the expressions, equivalent to Eqs. (1), (9) and (2), which define the corresponding local distribution of the height function obtained from the distance function to the interface, H^{LS} (Eq. (A1)), the corrected distribution $H^{LS(*)}$ (Eq. (A2)) and the curvature (Eq. (A3)), respectively.

5. Discussion of results

5.1. Height function computed from VOF distribution

5.1.1. Static tests

Fig. 6(a) and (b) shows the curvature errors for circular and spherical interfaces, respectively, obtained from the height function distribution H^{VOF} and from the corrected distribution $H^{VOF(*)}$. The notable improvement in the curvature computation accuracy achieved with the height function correction introduced in Eq. (9) can be observed by comparing the pictures on the left and right hand sides of Fig. 6(a) and (b). The effectiveness of the proposed method can also be assessed by comparing the curvature errors obtained from the corrected distribution $H^{VOF(*)}$ (open squares) and from the exact distribution H^{exact} (pictures at the right in Fig. 6(a) and (b)).

The global accuracy of the computed interface curvature is measured using the L_∞ and L_1 error norms, defined as

$$E_{L\infty} = \max(|\kappa - \kappa_{\text{exact}}|), \tag{11}$$

$$E_{L1} = \frac{\sum_i^n |\kappa - \kappa_{\text{exact}}|}{n}, \tag{12}$$

where n is the number of interfacial cells. Tables 1 and 2 show, respectively, the errors obtained for a circle of radius unity and for a one-dimensional cosine wave defined as in [4], with two different wavelengths, λ, and an amplitude equal to 1 (the interface curvature varies from $(2\pi/\lambda)^2$ to $-(2\pi/\lambda)^2$), in an 8^2 domain, using grid sizes of between 80^2 and 320^2 cells. Table 3 shows the errors for a sphere of radius 2 in an 8^3 domain and grid sizes of between 40^3 and 160^3 cells. In order to avoid favorable situations and to obtain results that are representative of the possible situations with different relative alignments and locations between grid and interface normals, the above error norms are averaged over 100 different cases obtained by randomly changing the location of the fluid bodies in the domain (for example, when the spherical shape is centered in the computational domain, γ is taken from Eq. (5) and the distribution $H^{VOF(*)}$ is used, the maximum errors obtained for the coarsest, intermediate and finest grids considered in Table 3 are, respectively, $7.47 \times 10^{-3}, 2.38 \times 10^{-3}$ and 4.86×10^{-4}, values which are considerably smaller than those presented in the table). It can be observed from Tables 1–3 that a considerable improvement in accuracy is obtained both in the 2D and 3D cases when the curvature is calculated from the corrected height function distribution $H^{VOF(*)}$ instead of H^{VOF}. It should also be pointed out that the improvement observed for the cosine wave cases of Table 2 is somewhat smaller than that observed in Table 1. This is due to the fact that the highest errors are produced at the interface points of higher curvature, which correspond to values of θ close to zero, for which, as can be observed from Fig. 6(a), the improvement in accuracy achieved by using the corrected $H^{VOF(*)}$ distribution is lowest. This behavior is illustrated in Fig. 7, where the interface curvature errors obtained from the H^{VOF}, $H^{VOF(*)}$ and H^{exact} distributions are represented as a function of θ, for a case with $\lambda = 8$ and $h = 0.05$. The effectiveness of using the corrected $H^{VOF(*)}$ distribution can be clearly observed from the figure. Note that the difference between the errors obtained using H^{VOF} and $H^{VOF(*)}$ is greatest for interface points with θ values close to zero, a value at which $|\kappa|$ is maximum and equal to $\pi^2/16$. As θ approaches 0.67 rad, the interface curvature rapidly decreases to zero, making the differences between both types of results progressively less relevant. Nevertheless, this test also demonstrates the good performance of the proposed height function correction technique in cases with variable interface curvature. When $\lambda = 2$, the interface curvature has a maximum value of π^2, which makes

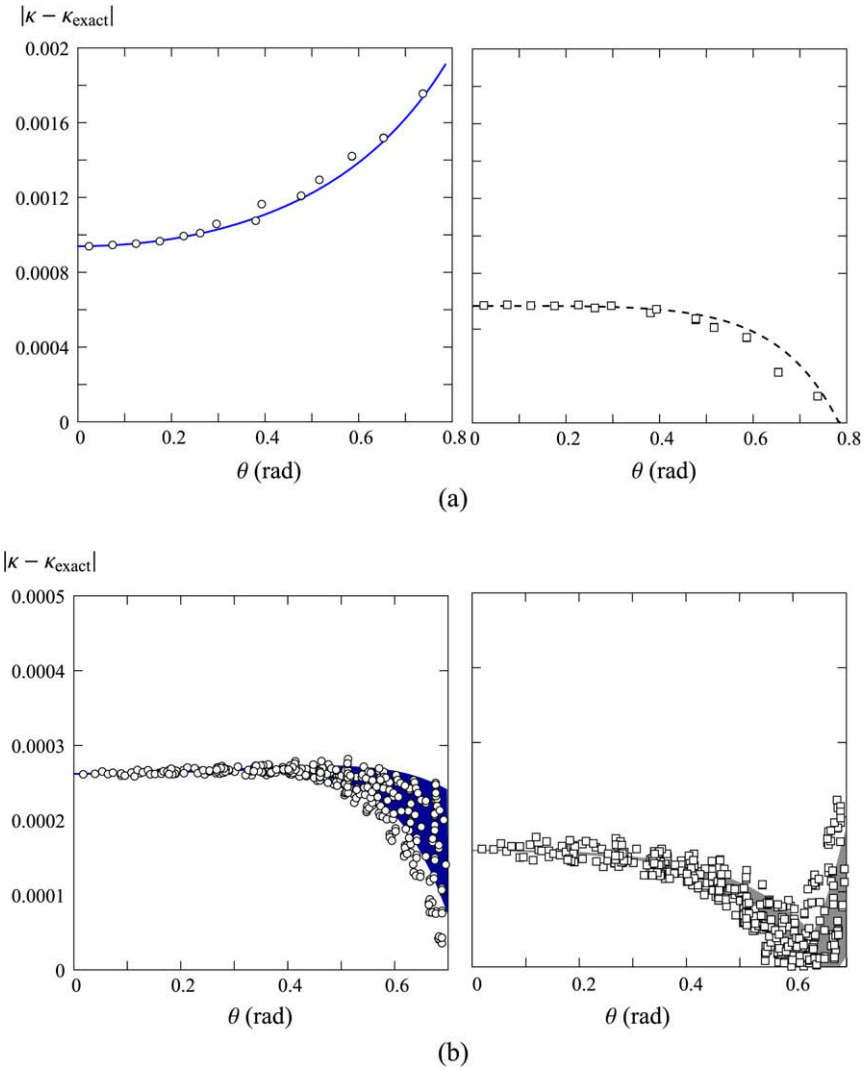

Fig. 6. Interface curvature errors obtained from the height function distribution H^{VOF} (open circles; pictures at the left) and from the corrected distribution $H^{VOF(*)}$ (open squares; pictures at the right), with a grid cell size $h = 0.05$: (a) circular interface of radius unity and (b) spherical interface of radius 2. Blue solid line and shaded area in pictures at the left denote curvature errors obtained from H^h; dashed line and grey shaded area in pictures at the right denote errors obtained from H^{exact}. (For interpretation of references to color in this legend Fig. 6, the reader is referred to the web version of this article.)

Table 1
Maximum and average curvature errors, $E_{L\infty}$ and E_{L1}, and convergence order, $\mathcal{O}$, for a circular interface of radius unity in a domain of size 8^2 (averaged values obtained over 100 random locations of the circle in the domain).

Grid cell size, h	Curvature computed from H^{VOF}				Curvature computed from $H^{VOF(*)}$			
	$E_{L\infty}$	$\mathcal{O}$	E_{L1}	$\mathcal{O}$	$E_{L\infty}$	$\mathcal{O}$	E_{L1}	$\mathcal{O}$
0.1	8.43×10^{-3}		5.00×10^{-3}		3.12×10^{-3}		1.94×10^{-3}	
		2.1		2.0		2.3		1.9
0.05	1.91×10^{-3}		1.22×10^{-3}		6.33×10^{-4}		5.04×10^{-4}	
		1.9		2.0		1.8		1.9
0.025	5.24×10^{-4}		3.04×10^{-4}		1.80×10^{-4}		1.31×10^{-4}	

$1/\kappa_{max}h$ relatively low and thus the smallest length scale to be poorly resolved for all the grid resolutions considered in Table 2 (a similar observation was made in [4] for this test). Note that, in this case, the effectiveness of using $H^{VOF(*)}$ instead of H^{VOF} for improving the accuracy of curvature computation decreases as the grid becomes coarser and the interface more poorly resolved, a trend which is more evident in the $E_{L\infty}$ error.

Table 2
Maximum and average curvature errors, $E_{L\infty}$ and E_{L1}, and convergence order, $\mathcal{O}$, for a cosine wave of different wavelengths and amplitude unity, in a domain of size 8^2 (averaged values obtained over 100 random locations of the fluid body in the domain).

Grid cell size, h	Curvature computed from H^{VOF}				Curvature computed from $H^{VOF(*)}$			
	$E_{L\infty}$	$\mathcal{O}$	E_{L1}	$\mathcal{O}$	$E_{L\infty}$	$\mathcal{O}$	E_{L1}	$\mathcal{O}$
	Wavelength $\lambda = 8$							
0.1	4.76×10^{-4}		1.18×10^{-4}		3.18×10^{-4}		8.81×10^{-5}	
		2.0		2.0		2.0		2.0
0.05	1.20×10^{-4}		3.00×10^{-5}		8.08×10^{-5}		2.23×10^{-5}	
		1.8		1.9		1.7		1.8
0.025	3.34×10^{-5}		8.03×10^{-6}		2.54×10^{-5}		6.47×10^{-6}	
	Wavelength $\lambda = 2$							
0.1	1.29×10^{0}		8.52×10^{-2}		1.29×10^{0}		8.05×10^{-2}	
		0.5		1.4		0.5		1.5
0.05	8.87×10^{-1}		3.19×10^{-2}		8.83×10^{-1}		2.75×10^{-2}	
		2.6		2.4		2.8		2.5
0.025	1.43×10^{-1}		6.06×10^{-3}		1.30×10^{-1}		4.88×10^{-3}	

Table 3
Maximum and average curvature errors, $E_{L\infty}$ and E_{L1}, for a sphere of radius 2 in a domain of size 8^3 (averaged values obtained over 100 random locations of the sphere in the domain). The convergence orders are in parentheses.

Grid cell size, h	Curvature from H^{VOF} ($\gamma = 0$)		Curvature from H^{VOF} (γ from Eq. (5))		Curvature from $H^{VOF(*)}$ (γ from Eq. (5))	
	$E_{L\infty}$	E_{L1}	$E_{L\infty}$	E_{L1}	$E_{L\infty}$	E_{L1}
0.2	6.86×10^{-2}	4.88×10^{-3}	1.28×10^{-2}	3.68×10^{-3}	1.33×10^{-2}	2.14×10^{-3}
	(2.3)	(2.1)	(2.0)	(2.1)	(2.1)	(2.1)
0.1	1.40×10^{-2}	1.12×10^{-3}	3.16×10^{-3}	8.82×10^{-4}	3.10×10^{-3}	4.90×10^{-4}
	(2.1)	(2.0)	(1.9)	(2.0)	(1.8)	(2.0)
0.05	3.27×10^{-3}	2.72×10^{-4}	8.49×10^{-4}	2.18×10^{-4}	8.60×10^{-4}	1.20×10^{-4}

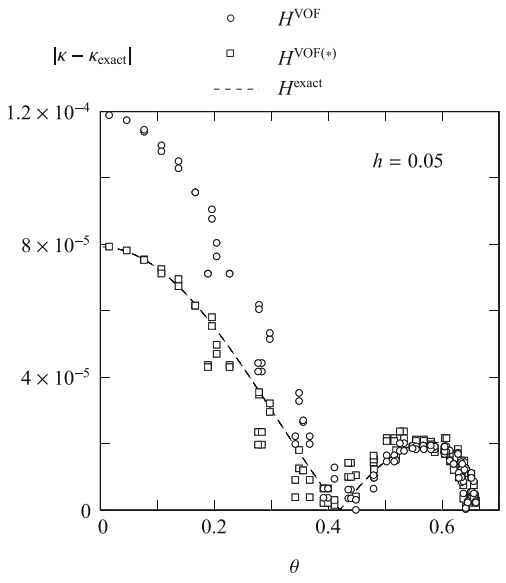

Fig. 7. Interface curvature errors obtained from H^{VOF} (open circles) and $H^{VOF(*)}$ (open squares) as a function of θ for a cosine wave of wavelength 8 and amplitude unity, in a domain of size 8^2, using a grid size $h = 0.05$. The results obtained from H^{exact} are depicted with a dashed line.

The results presented in Figs. 5 and 6 reveal that the accuracy of the proposed HF technique in computing the interface curvature mainly depends on the interface orientation and is relatively independent of the local volume fraction. This can be more clearly seen in Fig. 8, in which the interface curvature errors obtained from the $H^{VOF(*)}$ distribution and using smoothed

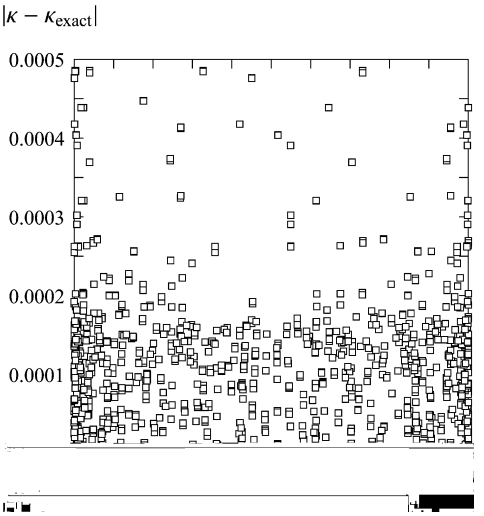

Fig. 8. Interface curvature errors as a function of F for the case of Fig. 6(b). Results obtained for $H^{VOF(*)}$ and γ given by Eq. (5).

partial derivatives are represented as a function of the volume fraction for the case of Fig. 6(b). Note that, even for near-homogeneous mixed cells (mixed cells with values of the volume fraction close to zero or one), there is no clear dependence of the curvature error on F.

Regarding the efficiency of the proposed model, the use of the corrected height function distribution in 3D cases increases the CPU time by about a 30% (the increase is considerably smaller in 2D), which is a reasonable cost given the increased accuracy achieved (all tests were run on a laptop with an Intel T9550 processor).

5.1.2. Surface tension-driven flow tests

The performance of the proposed technique in combination with a flow solver [10] has also been assessed using a static inviscid spherical drop test [23] and a drop oscillation test. In both cases, zero gravity and the same test conditions of Ref. [14] are assumed. The interface curvature at interfacial cell faces is obtained using the interpolation procedure described in [14]. The errors involved in any interpolation procedure used to obtain the interface curvature at locations different from interfacial cell centers will not be considered in this work.

Since the flow solver exactly balances the pressure gradient and surface tension force [6], any velocity field produced in the static drop test is solely due to interface curvature errors, and so the curvature calculation becomes the relevant point. In this test, a spherical drop of radius $R = 2$, centered in a domain of size 8^3, is considered. The densities inside and outside the drop are $\rho_1 = 1$ and $\rho_2 = 0.1$, and the surface tension coefficient $\sigma = 73$. The initial pressure and velocity are set equal to zero in the whole domain. Three different grid sizes and a time step Δt of 0.001, which satisfies the capillary constraint given by $\Delta t \leqslant [(\rho_1 + \rho_2)h^3/4\pi\sigma]^{1/2}$ for all the grid resolutions considered, are used. The spurious currents are estimated by the maximum velocity in the computational domain, $|\boldsymbol{u}|_{max}$.

Table 4 shows the $|\boldsymbol{u}|_{max}$ values after 1 and 50 time steps, and the averaged $|\boldsymbol{u}|_{max}$ value over the first 50 time steps, obtained from the H^{VOF} distribution using $\gamma = 0.0$ in Eqs. (3) and (4), and from the H^{VOF} and the corrected $H^{VOF(*)}$ distributions

Table 4
Spurious currents in the inviscid static drop test. Results for the maximum velocity $|\boldsymbol{u}|_{max}$ obtained with three different grid sizes and $\Delta t = 0.001$.

Grid cell size, h	$\|\boldsymbol{u}\|_{max}$ at $t = \Delta t$	$\|\boldsymbol{u}\|_{max}$ at $t = 50\Delta t$	Averaged $\|\boldsymbol{u}\|_{max}$ over the first 50 time steps
	Curvature computed from H^{VOF}; standard partial derivatives ($\gamma = 0$)		
0.4	7.06×10^{-3}	1.42×10^{-1}	1.09×10^{-1}
0.2	4.42×10^{-3}	3.40×10^{-2}	3.67×10^{-2}
0.1	4.87×10^{-3}	8.30×10^{-3}	1.25×10^{-2}
	Curvature computed from H^{VOF}; smoothed partial derivatives (γ from Eq. (5))		
0.4	5.43×10^{-3}	1.62×10^{-1}	1.03×10^{-1}
0.2	2.50×10^{-3}	2.52×10^{-2}	2.45×10^{-2}
0.1	1.31×10^{-3}	2.91×10^{-3}	2.94×10^{-3}
	Curvature computed from the corrected $H^{VOF(*)}$; smoothed partial derivatives (γ from Eq. (5))		
0.4	5.00×10^{-3}	1.50×10^{-1}	9.40×10^{-2}
0.2	2.32×10^{-3}	2.03×10^{-2}	1.99×10^{-2}
0.1	1.24×10^{-3}	4.28×10^{-3}	2.45×10^{-3}

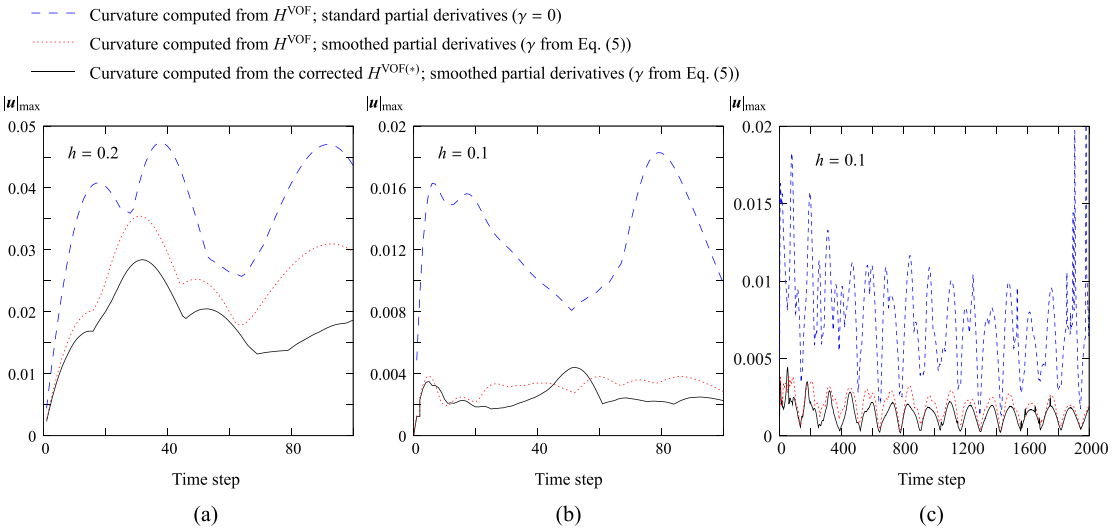

Fig. 9. Spurious currents in the inviscid static drop test. Results for the maximum velocity $|\boldsymbol{u}|_{max}$ as a function of time, obtained with $\Delta t = 0.001$ and two different grid sizes: (a) $h = 0.2$, (b) $h = 0.1$ and (c) $h = 0.1$ and a longer simulation time.

using γ obtained from Eq. (5), using grid sizes of between 20^3 and 80^3 cells. The increase in accuracy achieved by using smoothed partial derivatives of the height function to calculate the curvature and the further improvement obtained when the corrected $H^{VOF(*)}$ distribution is used can be observed from the table. The magnitude of the spurious currents decreases with grid refinement, with a convergence of around first order after one time step and of almost third order after 50 time steps. The improvement can be observed more clearly in the averaged error of the last column in the table, since the oscillations of $|\boldsymbol{u}|_{max}$ with time, shown in Fig. 9 for two different grid sizes, may make the comparison at certain instants less representative, as occurs at $t = 50\Delta t$ when $h = 0.1$. The asymptotic behavior of the spurious currents obtained for longer simulation times and $h = 0.1$ is shown in Fig. 9(c). When curvature is computed from the $H^{VOF(*)}$ distribution and using the γ values given by Eq. (5), it can be observed from the figure that $|\boldsymbol{u}|_{max}$ oscillates around an average value of 1.42×10^{-3}, with a wavelength of around 130, and that the amplitude of the oscillation gradually decreases with time, but more rapidly during the first 600 time steps. When using the H^{VOF} distribution, $|\boldsymbol{u}|_{max}$ oscillates with almost the same wavelength and a slightly higher amplitude around an average value of 1.95×10^{-3} when γ given by Eq. (5) is used, and more irregularly and around an average value of 7.55×10^{-3} when γ is taken as zero.

In the drop oscillation test we consider the oscillation with no external forces of a viscous drop, initially perturbed from its spherical shape and centered in a domain of size 4^3. The radius of the initial interface surface is given by $R = R_0[1 + \eta P_2(\cos\phi)]$, where $0 \leqslant \phi \leqslant \pi$ is the polar angle, $R_0 = 1$ is the radius of the spherical drop at equilibrium, $\eta = 0.01$ is the amplitude of the initial disturbance, and P_2 is the Legendre polynomial of order 2. The densities inside and outside the drop are $\rho_1 = 1$ and $\rho_2 = 0.01$, the corresponding viscosities are $\mu_1 = 1 \times 10^{-2}$ and $\mu_2 = 1 \times 10^{-4}$, and the surface tension coefficient is $\sigma = 1$. The time step $\Delta t = 0.35[(\rho_1 + \rho_2)h^3/4\pi\sigma]^{1/2}$ was used in all the simulations presented below [14]. The linear, irrotational approximation for the angular frequency of the drop oscillation derived by Lamb [11] is given by

$$w^2 = \frac{24\sigma}{R_0^3[3\rho_1 + 2\rho_2]}.$$

Fig. 10 shows the percentage error for the first oscillation period, T, defined as $|T - T^*| \times 100/T^*$, where $T^* = 2\pi/w$, as a function of grid size, obtained using the same three procedures and settings used in the static drop test. Besides the improvement in accuracy achieved by using the smoothed discretization of the partial derivatives of H^{VOF}, it can be observed that the use of the proposed $H^{VOF(*)}$ distribution substantially reduces the error involved, especially for fine grids. The first oscillation period obtained with the finest grid compares favorably with the value reported by Aulisa et al. [2] in their Table 5, which was obtained from a 3D-axisymmetric computation. The results obtained in the same drop oscillation test but with $\mu_1 = 5 \times 10^{-3}$ and $\sigma = 0.5$, computing the interface curvature from the corrected $H^{VOF(*)}$ distribution and using γ given by Eq. (5), have also been compared with those obtained from a 3D-axisymmetric computation by Sussman and Puckett [21] and Aulisa et al. [2]. For a grid cell size $h = 0.05$, we obtain $T = 3.166$ (the T^* value obtained from Lamb's theory is 3.152) with a convergence order of 2.5, which compares favorably with the results reported in [21,2], obtained with an equivalent grid size.

5.2. Height function computed from the distance function to the interface

Fig. 12(a) shows the height function error $|H^{LS} - H^{exact}|$, obtained analytically for different values of the distance from the considered cell to a circular interface, ϕ_j (see Fig. 11), as a function of θ. Note that the error not only depends on the interface

Fig. 11. Calculation of the approximate height function H^{LS} from a distance function distribution, for a circular interface of radius R.

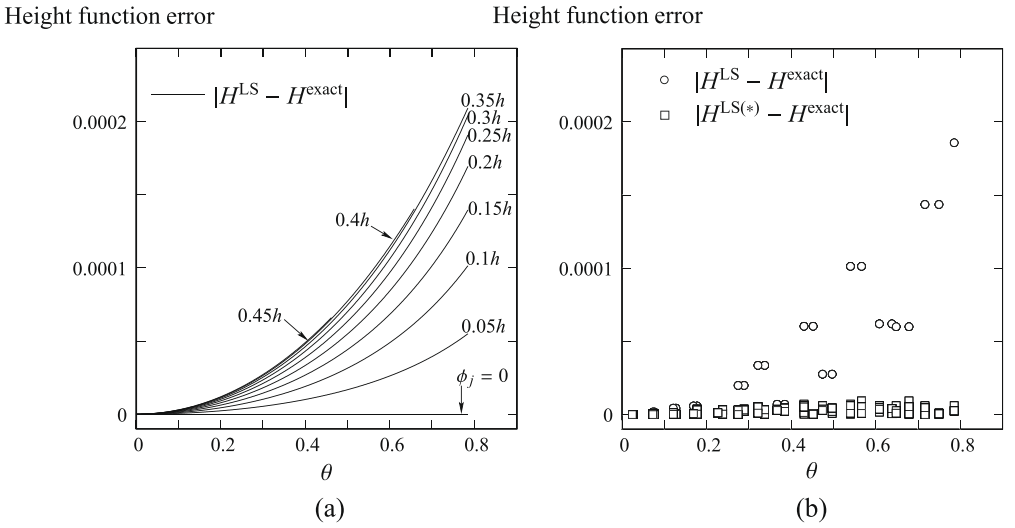

Fig. 12. Level set-based height function errors as a function of θ: (a) analytical results for a circular interface and different values of the distance from the cell to the interface and (b) results for a circular interface with $R = 1$, centered in a domain of size 8^2, obtained with a grid size $h = 0.05$. Only results that satisfy the condition $|\phi_j| > |\phi_{j+1}|$ in the example of Fig. 11 are represented.

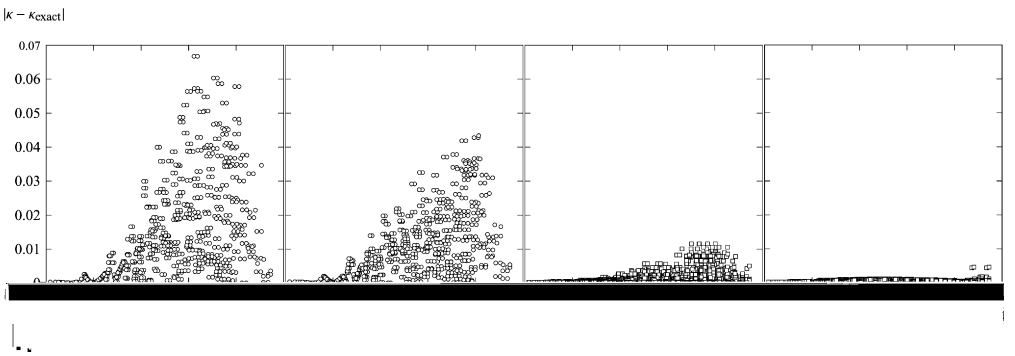

Fig. 13. Interface curvature errors as a function of θ obtained for a spherical interface with $R = 2$, centered in the domain, using a grid size $h = 0.05$. Results obtained from (a) H^{LS} and $\gamma = 0.0$; (b) H^{LS} and $\gamma = 0.2$; (c) $H^{LS(*)}$ and $\gamma = 0.2$ after one iteration; (d) $H^{LS(*)}$ and $\gamma = 0.2$ after eight iterations.

Table 5
Maximum and average curvature errors, $E_{L\infty}$ and E_{L1}, and convergence order, $\mathcal{O}$, computed from the level set-based H^{LS} and $H^{LS(*)}$ height function distributions, for a circular interface of radius unity and a spherical interface of radius 2, in a domain of size 8^2 and 8^3, respectively (averaged values obtained over 100 random locations of the fluid bodies in the domain). Smoothed finite difference approximations with $\gamma = 0.2$ are used for all the 3D results.

Grid cell size, h	Curvature computed from H^{LS}				Curvature computed from $H^{LS(*)}$			
	$E_{L\infty}$	$\mathcal{O}$	E_{L1}	$\mathcal{O}$	$E_{L\infty}$	$\mathcal{O}$	E_{L1}	$\mathcal{O}$
	Circle							
0.1	3.32×10^{-2}		1.11×10^{-2}		5.87×10^{-3}		2.70×10^{-3}	
		−0.3		0.1		1.2		1.5
0.05	3.95×10^{-2}		1.01×10^{-2}		2.52×10^{-3}		9.84×10^{-4}	
		−0.1		0.1		1.1		1.2
0.025	4.20×10^{-2}		9.34×10^{-3}		1.15×10^{-3}		4.21×10^{-4}	
	Sphere							
0.2	5.36×10^{-2}		1.20×10^{-2}		2.13×10^{-2}		3.67×10^{-3}	
		−0.2		0.1		1.8		1.8
0.1	5.97×10^{-2}		1.12×10^{-2}		5.91×10^{-3}		1.06×10^{-3}	
		0.0		0.0		2.0		1.4
0.05	6.09×10^{-2}		1.11×10^{-2}		1.49×10^{-3}		3.99×10^{-4}	

computed from $H^{LS(*)}$ of Table 5 are larger than those of Tables 1 and 3, especially for fine grids. However, it should be mentioned that, when the exact values of $\boldsymbol{n}_{r,s}$ are used in Eq. (A2), second-order accuracy is achieved and the errors obtained using $H^{LS(*)}$ become very close to those of Table 1, and only slightly larger than those of Table 3. This means that a more accurate calculation of the interface normal used in Eq. (A2) would probably lead the level set and VOF-based approaches of the proposed height function technique to have a similar level of accuracy.

6. Conclusions

An analysis of the errors involved in the computation of interface curvature from volume fraction distributions has been carried out, leading to an improved version of the height function technique. The improvement is based on introducing a correction of the height function discretization error estimated from the local osculating spheres constructed at interface points. The notable increase in accuracy of the interface curvature computation that can be efficiently obtained using the proposed error correction and a smoothed discretization of the partial derivatives of the height function has been demonstrated through several tests.

Acknowledgments

The authors gratefully acknowledge the support of the Spanish Ministerio de Educación y Ciencia under grants DPI2006–07047 and DPI2007–63275, and the Spanish Fundación Séneca (Agencia de Ciencia y Tecnología de la Región de Murcia) under grant 05802/PI/07.

Appendix A. Computation of curvature using a HF distribution obtained from the distance function

Consider a cell (i,j,k) that satisfies the condition $\phi_{i,j,k}\phi_{i,j,k+1} < 0$. Following considerations similar to those used in Section 2, an approximate local HF value at the cell can be computed from the ϕ distribution using the following simple interpolation ($\phi > 0$ inside the fluid):

$$H^{LS}_{r,s} = \frac{\phi_{i+r,j+s,k(r,s)}}{\phi_{i+r,j+s,k(r,s)} - \phi_{i+r,j+s,k(r,s)+1}} h - (k - k(r,s))h, \quad \text{for } r = -1,0,1 \quad \text{and} \quad s = -1,0,1, \tag{A1}$$

where $k(r,s)$ is the index between $k+3$ and $k-3$, which satisfies the following conditions: $\text{sign}(\phi_{i+r,j+s,k(r,s)}) = \text{sign}(\phi_{i,j,k})$ and $\phi_{i+r,j+s,k(r,s)}\phi_{i+r,j+s,k(r,s)+1} < 0$. Note that the heights defined by Eq. (A1) are relative to the height kh of cell (i,j,k).

As shown in Section 5.2, with the simple interpolation given by Eq. (A1) the interface curvature does not converge as the grid becomes more refined. A similar finding was reported by Sussman and Ohta [20] for height functions generated from the signed distance to the reconstructed VOF interface. These authors proposed a method that overcomes this drawback and performs as well as the VOF height function approach to discretize curvature, claiming that it is even more accurate, especially when two interfaces are in close proximity to each other. In this work, an expression equivalent to Eq. (9), which can be easily deduced in view of the 2D example of Fig. 11, is used to improve the accuracy of the local height function distribution:

$$H^{LS(*)}_{r,s} = \left| \left[\frac{\chi^2}{\kappa^2_{r,s}} - \left(n^2_{x(r,s)} + n^2_{y(r,s)} \right) \left(\frac{\chi}{\kappa_{r,s}} + \phi_{i+r,j+s,k(r,s)} \right)^2 \right]^{1/2} - \left[\left(1 - n^2_{x(r,s)} - n^2_{y(r,s)} \right) \left(\frac{\chi}{\kappa_{r,s}} + \phi_{i+r,j+s,k(r,s)} \right)^2 \right]^{1/2} \right| - (k - k(r,s))h, \tag{A2}$$

where $\chi = 2$ for 3D and $\chi = 1$ for 2D. The first term on the right hand side is the exact height function referring to the center of the osculating sphere of radius $\chi/|\kappa_{r,s}|$ (note that $\kappa_{r,s}$ is negative when the center of curvature lies in the fluid) at the interface point closest to cell $(i+r, j+s, k(r,s))$, where the interface orientation, given by $\boldsymbol{n}_{r,s} \equiv (n_{x(r,s)}, n_{y(r,s)}, n_{z(r,s)})$, is obtained using standard second-order finite difference approximations at cell $(i+r, j+s, k(r,s))$. The second term is the height of the center of the cell $(i+r, j+s, k(r,s))$ from the center of the osculating sphere (H^{ref} in the case of Fig. 11). When the maximum component of $\boldsymbol{n}_{r,s}$ does not coincide with that of $\boldsymbol{n}_{0,0}$, the curvature $\kappa_{r,s} = \kappa_{0,0}$.

When the HF is obtained from Eq. (A1) or Eq. (A2), the curvature of the interface is determined as

$$\kappa = \text{sign}(n_z) \frac{H_{xx} + H_{yy} + H_{xx}H_y^2 + H_{yy}H_x^2 - 2H_{xy}H_xH_y}{\left(1 + H_x^2 + H_y^2\right)^{3/2}}. \tag{A3}$$

References

[1] S. Afkhami, M. Bussmann, Height functions for applying contact angles to 2D VOF simulations, Int. J. Numer. Method Fluids 57 (2008) 453–472.
[2] E. Aulisa, S. Manservisi, R. Scardovelli, A novel representation of the surface tension force for two-phase flow with reduced spurious currents, Comput. Method Appl. Mech. Eng. 195 (2006) 6239–6257.
[3] A.J. Chorin, Curvature and solidification, J. Comput. Phys. 57 (1985) 472–490.
[4] S.J. Cummins, M.M. Francois, D.B. Kothe, Estimating curvature from volume fractions, Comput. Struct. 83 (2005) 425–434.

[5] S.V. Diwakar, S.K. Das, T. Sundararajan, A quadratic spline based interface (QUASI) reconstruction algorithm for accurate tracking of two-phase flows, J. Comput. Phys. 228 (2009) 9107–9130.
[6] M.M. Francois, S.J. Cummins, E.D. Dendy, D.B. Kothe, J.M. Sicilian, M.W. Williams, A balanced-force algorithm for continuous and sharp interfacial surface tension models within a volume tracking framework, J. Comput. Phys. 213 (2006) 141–173.
[7] M.M. Francois, B.K. Swartz, Interface curvature via volume fractions, heights, and mean values on nonuniform rectangular grids, J. Comput. Phys. 229 (2010) 527–540.
[8] I. Ginzburg, G. Wittum, Two-phase flows on interface refined grids modeled with VOF, staggered finite volumes, and spline interpolants, J. Comput. Phys. 166 (2001) 302–335.
[9] J. Helmsen, P. Colella, E.G. Puckett, Non-convex profile evolution in two dimensions using volume of fluids, Technical Report LBNL-40693, Lawrence Berkeley National Laboratory, 1997.
[10] J. Hernández, J. López, P. Gómez, C. Zanzi, F. Faura, A new volume of fluid method in three dimensions. Part I: multidimensional advection method with face-matched flux polyhedra, Int. J. Numer. Method Fluids 58 (2008) 897–921.
[11] H. Lamb, Hydrodynamics, Cambridge University Press, Cambridge, 1932.
[12] J. López, J. Hernández, P. Gómez, F. Faura, A volume of fluid method based on multidimensional advection and spline interface reconstruction, J. Comput. Phys. 195 (2004) 718–742.
[13] J. López, J. Hernández, Analytical and geometrical tools for 3D volume of fluid methods in general grids, J. Comput. Phys. 227 (2008) 5939–5948.
[14] J. López, C. Zanzi, P. Gómez, R. Zamora, F. Faura, J. Hernández, An improved height function technique for computing interface curvature from volume fractions, Comput. Method Appl. Mech. Eng. 198 (2009) 2555–2564.
[15] D. Lörstad, M.M. Francois, W. Shyy, L. Fuchs, Assessment of volume of fluid and immersed boundary methods for droplet computations, Int. J. Numer. Method Fluids 46 (2004) 109–125.
[16] M. Malik, E.S.-C. Fan, M. Bussmann, Adaptive VOF with curvature-based refinement, Int. J. Numer. Method Fluids 55 (2007) 693–712.
[17] Y. Renardy, M. Renardy, PROST: a parabolic reconstruction of surface tension for the volume-of-fluid method, J. Comput. Phys. 183 (2002) 400–421.
[18] M. Sussman, A second order coupled level set and volume-of-fluid method for computing growth and collapse of vapor bubbles, J. Comput. Phys. 187 (2003) 110–136.
[19] M. Sussman, M. Ohta, High-order techniques for calculating surface tension forces, Int. Ser. Numer. Math. 154 (2007) 425–434.
[20] M. Sussman, M. Ohta, A stable and efficient method for treating surface tension in incompressible two-phase flow, SIAM J. Sci. Comput. 31 (2009) 2447–2471.
[21] M. Sussman, E.G. Puckett, A coupled level set and volume-of-fluid method for computing 3D and axisymmetric incompressible two-phase flows, J. Comput. Phys. 162 (2000) 301–337.
[22] M. Torrey, L. Cloutman, R. Mjolsness, C. Hirt, NASA-VOF2D: a computer program for incompressible flows with free surfaces, Technical Report LA-10612-MS, Los Alamos National Laboratory, 1985.
[23] M.W. Williams, D.B. Kothe, E.G. Puckett, Convergence and accuracy of continuum surface tension models, in: W. Shyy, R. Narayanan (Eds.), Fluid Dynamics at Interface, Cambridge University Press, Cambridge, 1999, pp. 294–305.
[24] D.L. Youngs, An interface tracking method for a 3D Eulerian hydrodynamics code, Technical Report 44/92/35, AWRE, 1984.
[25] VOFTools, a package of FORTRAN subroutines with analytical and geometrical tools for 2D/3D VOF methods in general grids. Available from: <http://www.dimf.upct.es/personal/lrj/voftools.html>.